

# Transport barriers and edge localized modes-like bursts in a plasma model with turbulent equipartition profiles

V. Naulin<sup>a)</sup> and J. Juul Rasmussen

Association EURATOM-Risø National Laboratory, Optics and Fluid Dynamics Department, OFD-128 Risø, 4000 Roskilde, Denmark

J. Nycander

Department of Meteorology, University of Stockholm, 106 91 Stockholm, Sweden

(Received 13 November 2002; accepted 20 January 2003)

Self-consistent development of transport barriers is investigated analytically and numerically in flux driven interchange turbulence with highly intermittent turbulent fluxes. Numerical simulations on a bounded domain show turbulence leading to a homogenization of Lagrangian invariants by mixing, resulting in quasisteady pressure profiles predicted by turbulent equipartition. Below a critical aspect ratio  $\alpha = L_y/L_x$ —for our parameters  $\approx 3.8$ —which is related to the rotational transform, large scale poloidal flows develop. They reduce the energy in the turbulence, prevent mixing, and constitute transport barriers for the turbulent fluxes, but are intermittently disrupted by strong bursts in the transport, which may be related to the strong edge localized modes observed in toroidal devices.

© 2003 American Institute of Physics. [DOI: 10.1063/1.1559993]

## I. INTRODUCTION

The generation of large scale flows by the rectification of small scale turbulent fluctuations is of great importance in fluids, e.g., geophysical flows<sup>1</sup> and thermal convective flows,<sup>2</sup> as well as in magnetically confined plasmas.<sup>3</sup> The flows are important as they act back on the turbulence by shearing apart and thereby suppressing fluctuations on the transport scales, thus setting up transport barriers.

More specific in hot magnetized plasmas the main cross-field transport is anomalous, i.e., not diffusive in the classical sense, and ascribed to low frequency electrostatic fluctuations.<sup>4</sup> It is generally recognized that self-consistently developing large scale poloidal flows strongly reduce the radial turbulent transport by “quenching” the turbulence (see Refs. 3, 5, and references therein). This mechanism may be responsible for the rapid transition to an enhanced confinement in magnetically confined plasmas, e.g., the celebrated H-mode regime first observed in the ASDEX tokamak.<sup>6</sup> The H-mode<sup>7</sup> is often found to be accompanied by bursts in the transport, related to edge localized modes (ELM),<sup>8,9</sup> which go along with magnetohydrodynamic (MHD) activity, the so-called ELMy H-mode. If no such intermittent transport behavior is observed, rising pressure gradients often violently terminate the H-mode plasma by disruption.

Since neither turbulence nor the associated bursty transport can or should be avoided, it is essential to understand the interplay between poloidal flows resp. transport barriers on the one hand and turbulence as well as transport on the other hand. The ultimate goal will be to use this understanding to develop strategies for active control and regulation of the turbulent transport.

In the plasma context, efforts to describe self-consistent

poloidal flow generation by anisotropic turbulence were initiated by Diamond and Kim.<sup>10</sup> The flow is driven by the turbulence via the off-diagonal elements in the Reynolds stress tensor, i.e.,  $R_{uv} = \langle uv \rangle$ , where  $u$  and  $v$  are the radial and poloidal components of the fluctuating velocity. Previously Biglari *et al.*<sup>11</sup> had shown that a shear flow may act stabilizing on turbulent fluctuations via a decorrelation mechanism.

In the present work we consider the evolution and dynamics of transport barriers, in the form of poloidal flows, and the interplay with the turbulent transport, which reveal an intermittent behavior with very strong burst events. We have employed a self-consistent model for pressure driven electrostatic turbulence of a plasma in an inhomogeneous magnetic field. This is a rough model of the outboard side of a toroidal confinement device but includes the effects of unfavorable curvature in an energy preserving manner and describes the evolution of profiles as well as fluctuations.

The turbulence is sustained by a heat flux entering the system from the hot inside and leaving at the cold outside. A similar model was used in Ref. 12 to explore the formation of turbulent equipartition states, the so-called TEP-state,<sup>13</sup> achieved by the equipartition of Lagrangian invariants: This state determines the mean global behavior of the system if the invariants are sufficiently robust, that is they “survive” for times much longer than the system mixing time. The average profiles of density and temperature in the TEP state are close to the linear stability threshold. Note, however, that any turbulent mixing will arrange that these marginally stable profiles are reached, even from below and in the absence of sources. Theories including critical gradients normally rely on the system relaxing from a state with a gradient steeper than the critical one. TEP predicts thus up-gradient transport while it does not give nor rely on any information about the spatial character of the transport, as f.x. self orga-

<sup>a)</sup>Electronic mail: volker.naulin@risoe.dk

nized critical (SOC) transport models<sup>14</sup> do. The latter are characterized by a power law behavior of the probability distribution function of the transport and self-similar character of the turbulence. Systems showing TEP behavior might thus as well fulfill the characterizations for SOC. Here we, however, want to concentrate on the interplay between shear flow and the TEP state.

The TEP state only exists, as mentioned above, if the turbulent mixing is stronger than the viscous diffusion. Thus, if the turbulence is quenched in some way, the profiles will relax towards the state controlled by the diffusion terms and the time averaged profile in the driven case will be steeper than the marginal stable one.

For a specific parameter regime strong, sheared, poloidal flows are observed to be generated self-consistently by the turbulence. The aspect ratio,  $\alpha$ , of the domain seems to be the most important parameter and the poloidal flows are persistent for  $\alpha < \alpha_c$ . The flows quench the turbulence. That is, they transform the energy in the turbulent motion into ordered poloidal flow, which provides no cross field transport. Moreover the developing flows may stabilize the instability. Thus, the TEP profiles will no longer be sustained, and a steep pressure gradient builds up due to viscous diffusion. This gradient, which is usually steeper than the critical gradient for instability, appears to be stabilized by the poloidal flow. However, also the flow decays due to the lack of instability drive and can at some point no longer stabilize the steep gradients. This results in a burst of turbulence and transport on a time scale much shorter than the viscous time scale. The appearance of the bursts is quasiperiodic with a time separation related to the viscous time scale and they may be related to the ELM-like structures discussed above. We suggest that they may explain at least the class of the strong type I ELM's.<sup>8,9</sup> A similar behavior with strong intermittent bursts is commonly observed in convection problems.<sup>2</sup> See also Takayama *et al.*,<sup>15</sup> who employed a Boussinesq model to simulate interchange mode turbulence.

## II. MODEL EQUATIONS

Our model is based on the fluid equations and describes the fluid drifts accurately in the presence of an inhomogeneous, curved magnetic field. Included are the adiabatic compression and heating of fluid parcels being displaced into a region of higher magnetic field. Density and temperature profiles are allowed to evolve self-consistently under the influence of eventual external heating, and so is the background potential profile, corresponding to a mean flow,

$$\frac{\partial n}{\partial t} + \{ \phi, n \} + \mathcal{K}(n + T - \phi) = \nu \nabla^2 n, \quad (1)$$

$$\frac{\partial T}{\partial t} + \{ \phi, T \} + \frac{2}{3} \mathcal{K} \left( n + \frac{7}{2} T - \phi \right) = \kappa \nabla^2 T, \quad (2)$$

$$\frac{\partial \nabla^2 \phi}{\partial t} + \{ \phi, \nabla^2 \phi \} + \mathcal{K}(n + T) = \mu \nabla^4 \phi. \quad (3)$$

Here  $\{f, g\} = (\partial f / \partial x)(\partial g / \partial y) - (\partial g / \partial x)(\partial f / \partial y)$  denotes the Poisson bracket. The potential  $\phi$  is normalized by  $\mathcal{T}e$ , the time by  $\omega_{ci}^{-1} = m_i / (eB_0)$ , and the length by  $\rho = (\mathcal{T}m_i)^{1/2} / \omega_{ci}$ . The curvature operator,

$$\mathcal{K} = -\nabla \cdot \frac{\mathbf{B} \times \nabla}{B^2}.$$

The coefficients  $\nu$ ,  $\kappa$ , and  $\mu$  model the particle diffusion, the heat diffusion, and the viscosity, respectively. In the derivation of Eqs. (1)–(3) it is assumed that the fields deviate only slightly from reference levels  $\mathcal{N}$ ,  $\mathcal{T}$ , with, e.g.,  $\tilde{n} = \mathcal{N}(1 + n(x, y, t))$  or in other words the variation of the profiles is small compared to the absolute levels of the background quantities. Modeling the outboard midplane of a tokamak for a simplified nonsheared magnetic field configuration, the curvature operator reduces to  $\mathcal{K}(f) = \omega_B \partial f / \partial y$ , where  $\omega_B = 2\rho / R_0$ . This corresponds to the large aspect ratio approximation for the magnetic field  $\mathbf{B} = (B_0 R_0 / R) \hat{\mathbf{b}}$ , where  $\hat{\mathbf{b}}$  is the unit vector in the toroidal direction, locally along the  $z$ -coordinate.  $R$  is the distance from the torus axis and  $B_0$  is the magnetic field at  $R = R_0$ . In the coordinate system of the considered slab,  $x$  corresponds to the radial direction and  $y$  to the poloidal direction.

In the inviscid limit the equations possess the Lagrangian invariants,<sup>12</sup>

$$l_{\pm} = \pm \sqrt{5/2} (n + \omega_B x) + 3T/2 - n, \quad (4)$$

advected by the pseudovelocities

$$\mathbf{v}_{\pm} = \hat{z} \times \nabla [ \phi - n - (1 \pm (5/2)^{1/2}) T ].$$

If the turbulence can mix these invariants effectively over the available volume on a time scale much shorter than the viscous time scale, the Lagrangian invariants will on average be uniformly distributed. This leads to TEP profiles

$$\langle n \rangle + \omega_B x \approx \text{const} \quad \text{and} \quad \langle T \rangle + \frac{2}{3} \omega_B x \approx \text{const}, \quad (5)$$

where  $\langle \cdot \rangle$  denotes an ensemble average that we assume to be replaceable with an average over time and the periodic poloidal coordinate, i.e., flux surface average. Also in the inviscid limit Eqs. (1)–(3) conserve the energy-like integral,

$$E = \int \left[ \frac{1}{2} (\nabla \phi)^2 - (n + T) \omega_B x \right] dx dy. \quad (6)$$

The first term is the kinetic energy, while the second has the form of potential energy. It represents that part of the thermal energy which can be converted to kinetic energy when fluid parcels are displaced to a region with weaker magnetic field, which gives rise to instabilities. The approximations behind the derivation of Eqs. (1)–(3) are quite analogous to the classical Boussinesq approximation.<sup>16</sup> In usual fluid convection, thermal energy is converted to kinetic energy, but in the Boussinesq equations commonly used to describe such convection the energy equation only contains kinetic and potential energy, while heat is conserved separately, just like in Eqs. (1)–(3).

We should emphasize that in contrast to models, where curvature is modeled by an effective gravity—the resistive  $g$ -paradigm—the magnetic field inhomogeneity (correspond-

ing to curvature) here just couples the equations, i.e., it allows the potential energy in the pressure gradient to be converted to kinetic energy of the plasma. Thus, the field inhomogeneity does not act as a source of free energy itself.

To investigate the linear stability we linearize Eqs. (1)–(3) around the background profiles  $n_0(x)$ ,  $T_0(x)$  assuming a waveform for the potential perturbation  $\psi_k(x)\exp(iky - i\omega t)$  respecting the boundary conditions in the  $x$ -direction, and similarly for  $n$  and  $T$ , where  $k$  is the wave number in the  $y$ -direction. The equation for the wave amplitude  $\psi_k$  reads

$$\frac{d^2\psi_k}{dx^2} + [-k^2 + D(c, x)]\psi_k = 0, \quad (7)$$

where

$$D = \frac{cN - (5/3)(\omega_B)^2(n'_0 + \omega_B)}{c(c^2 - (10/3)c\omega_B + (5/3)\omega_B^2)}. \quad (8)$$

We have introduced  $c = \omega/k$ , and the “buoyancy” frequency

$$N \equiv \omega_B(n'_0 + T'_0 + \frac{5}{3}\omega_B).$$

Here the “prime” denotes derivative with respect to  $x$ .

Equation (7) may be solved as an eigenvalue problem for given profiles and with the boundary conditions,

$$\psi_k|_{(x=0)} = 0 \quad \text{and} \quad \psi_k|_{(x=L_x)} = 0,$$

resulting in an expression for the complex phase velocity  $c$ , the dispersion relation. Here  $L_x$  is the width of the slab in the radial direction. In order to illustrate the features of the instability we consider two simplified cases.

Within a local approximation and considering the long wave limit, i.e.,  $D \approx N/(c^2 - \frac{10}{3}c\omega_B + \frac{5}{3}\omega_B^2)$ , we obtain

$$c = \frac{5}{3}\omega_B \left( 1 - \frac{1}{2} \frac{n'_0 + \omega_B}{n'_0 + T'_0 + \frac{5}{3}\omega_B} \pm \sqrt{\frac{N}{K^2}} \right), \quad (9)$$

where  $K^2 = k_x^2 + k^2$ . Thus, we have instability for  $N < 0$ . This is the “standard” Rayleigh–Taylor instability with the growth rate

$$\gamma = k \sqrt{\frac{|N|}{K^2}}. \quad (10)$$

Furthermore with  $\text{Re}(c) = \frac{5}{3}\omega_B$  we have propagation in the  $y$  direction.

For the special case, where  $n_0$  and  $T_0$  are linear in  $x$ ,  $N$  becomes independent of  $x$ , and we can find the general solution of Eq. (7), that satisfies the boundary conditions,

$$\psi_k(x) = \sum A_n \sin \frac{n\pi x}{L_x}. \quad (11)$$

The dispersion relation for these modes is similar to the one given by Eq. (9) with  $K^2 = k^2 + (n\pi/L_x)^2$ , and it is readily seen that the “fundamental mode,”  $n=1$ , has the largest maximum growth rate,

$$\gamma = k \sqrt{\frac{|N|}{k^2 + (\pi/L_x)^2}}. \quad (12)$$

As was already emphasized, the TEP profile, as given by Eq. (5), is marginally stable.

### III. NUMERICAL RESULTS

The model equations are solved numerically using a finite difference code, based on the energy and enstrophy conserving third order discretization of the Poisson bracket,<sup>17</sup> which is also used to evaluate the curvature terms. For propagation in time we use a third order stiffly stable scheme as described in Ref. 18. We consider a two-dimensional domain which is bounded in  $x$  (the radial direction) with length  $L_x$  and periodic in  $y$  (the poloidal direction) with length  $L_y$ . The poloidal periodicity length may be interpreted as the recurrence length of a magnetic field line: Assuming an infinite correlation along magnetic field lines for the safety factor  $q=3$  rational surface we would find  $L_y = 2\pi r/3$  and for  $q=4$  the poloidal periodicity length would be  $L_y = 2\pi r/4$ . The aspect ratio of our slab-domain  $\alpha \equiv L_y/L_x$  will then be directly related to the safety factor  $q$ , i.e.,  $\alpha \propto 1/q$ . The exact value naturally depends on the radial length scale. Our simplified 2D model does, at the present state, not reflect the details of magnetic configuration, but it is known from linear analysis that ballooning modes—being made responsible for giant ELMs—are rather wide and have an extend of about 20% of the minor radius of the torus.<sup>19,20</sup> We will thus take the radial extend of these linear modes as an estimate on the radial scale length  $L_x$ . With a typical  $q$ -value at the edge of  $q=4$ , we then estimate an aspect ratio for our system of equations. We find an effective aspect ratio of  $\alpha = (2\pi/4) \times (1/0.2) \approx 8$ , which is of the same order of magnitude as we consider.

We would also like to point out that opposed to turbulent fluctuation simulations, we resolve both the fast time scales of the turbulence and the slow profile evolution time scale. Computational resources thus restrict our spatial resolution, necessitating artificially high values for viscosity and diffusivities as compared to experimental values, and finally dictate, for the time being, the use of a 2D model.

The diffusivities and dissipation coefficients,  $\nu$ ,  $\kappa$ ,  $\mu$  were chosen to be equal ( $= 10^{-3}$  in most of the runs). The source of energy to drive the turbulent fluctuations is an imposed temperature or pressure difference between the walls, using the boundary conditions  $T|_{x=0} = T_0$  and  $T|_{x=L_x} = 0$ . The diffusive particle flux at the walls was set to zero by prescribing  $\partial_x n|_{x=0, L_x} = 0$ , and the potential  $\phi$  was kept constant at the walls, so that the velocity component perpendicular to the walls vanished.

We performed numerical runs for various values of the different parameters of the system: the imposed temperature difference  $T_0$ , the aspect ratio  $\alpha \equiv L_y/L_x$ , the size of the system  $L_x$ , and the diffusivities and the dissipation coefficients. When  $T_0$  is sufficiently large to drive the instability, we observe the following general scenarios, depending on aspect ratio as visualized in Fig. 1:

- (a) For sufficiently large  $\alpha \geq \alpha_c \approx 3.8$  (for  $\nu = \kappa = \mu = 10^{-3}$ ) the system develops into the TEP state described in Eq. (5) regardless of the value of  $T_0$ , dem-

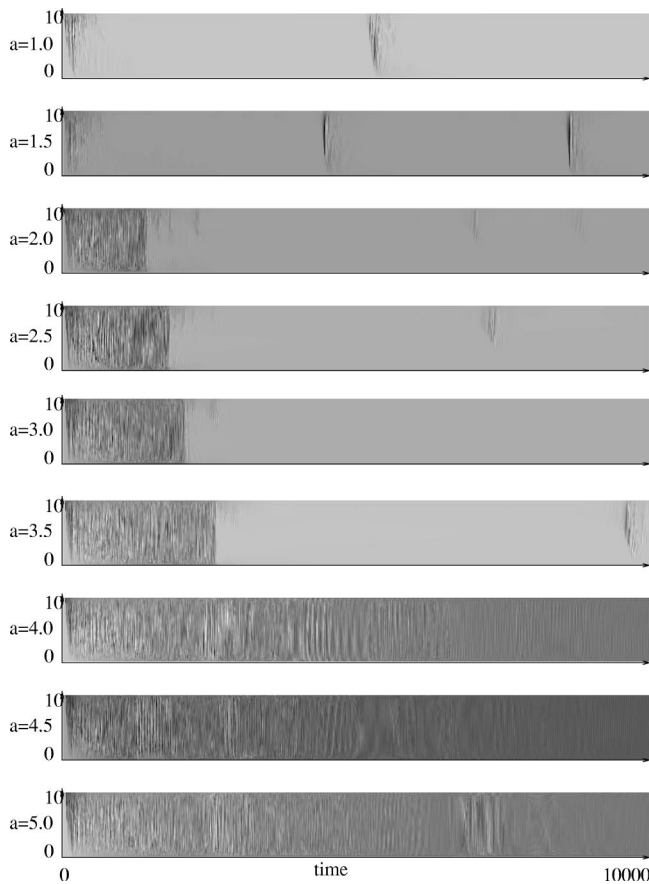


FIG. 1. Poloidally averaged heat flux vs time for different aspect ratios. For an aspect ratio larger than 3.8, no transport suppression is observed.

onstrating profile consistency and resilience.<sup>12</sup> There is a radial, turbulent heat flux, which is persistent, but intermittent.

- (b) For smaller  $\alpha$  a different behavior is observed. In an initial phase the turbulence develops and establishes the TEP profiles with a high flux-level. Later on, the flux is interrupted, that is, an H-mode-like state with steeper averaged gradients and lower effective diffusion coefficients develops. For long periods of time the system is very quiescent, as seen in Fig. 1 and detailed in Figs. 2(a) and 2(b) for  $\alpha = 1$ . However, sporadic flux bursts of high amplitude—analogue to ELMs—are observed to occur at somewhat random intervals. The time scale of the quiescent periods between the bursts is, however, related to the viscous time scale. Increasing the viscosity we observe that the average time intervals between the bursts decreases almost proportionally to  $\mu^{-1}$ , as illustrated in Fig. 2(b). Here the evolution of the heat flux is shown for  $\mu = 0.01$ , and the number of bursts is about 10 times larger than in Fig. 2(a). Increasing the viscosity even further we reach a value where the instability becomes too weak to drive a sufficient fluctuation level for establishing a TEP profile.

The quiet periods are associated with the establishment of a strong poloidal mean flow which characterizes the trans-

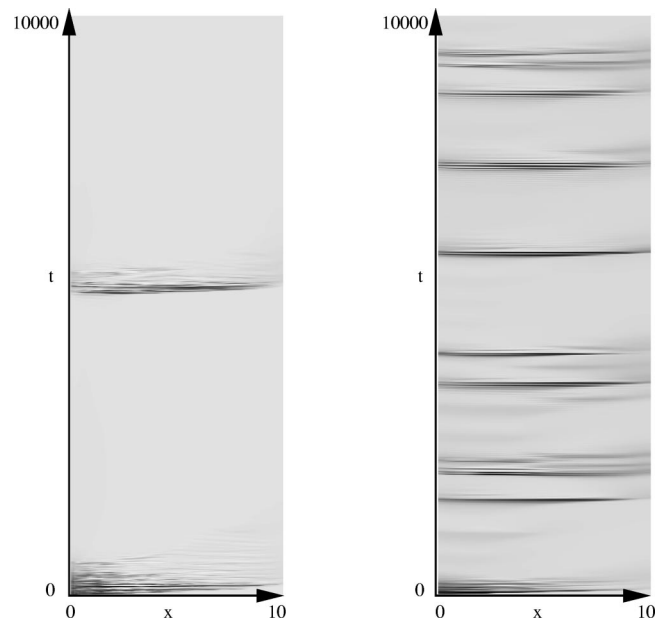


FIG. 2. Poloidally averaged heat flux  $\Gamma_T = \langle uT \rangle$  vs  $(x, t)$  for an aspect ratio  $\alpha = L_y/L_x = 1$  and dissipation coefficients  $\nu = \kappa = \mu = 10^{-3}$  (left frame) and  $10^{-2}$  (right frame). The gray-scale is from  $-0.2$  (light) to  $0.5$  (dark).

port barrier (see Fig. 3). This flow, which is strongly sheared and often only develops in a part of the domain, quenches the turbulence and acts as an effective barrier for transport and mixing. As there is no longer sufficient mixing by the turbulence to maintain the TEP profiles and the nonturbulent flux is much smaller than the turbulent one the profiles start to steepen via the diffusive inflow of heat from the hot boundary. We estimate the competition between the turbulent mixing and the diffusion by averaging Eq. (2) over  $y$ ,

$$\frac{\partial \langle T \rangle}{\partial t} = - \frac{\partial}{\partial x} \langle uT \rangle + \kappa \frac{\partial^2}{\partial x^2} \langle T \rangle. \tag{13}$$

Here  $u$  is the radial velocity component and  $\langle f \rangle = (1/L_y) \int_0^{L_y} f dy$  is the flux surface average. The turbulent heat flux  $\Gamma_T = \langle uT \rangle$  is proportional to the turbulence level; a quasilinear estimate using the local dispersion relation gives  $\Gamma_T \propto -(T'_0 + 2\omega_B/3) |\phi|^2$ . It is directly related to the instability mechanism, and by using Eq. (6) it is readily observed that  $\Gamma_T$  is responsible for transferring the free potential energy stored in the gradient into kinetic energy of the fluctuations. When  $\Gamma_T$  is stronger than the diffusive flux  $\kappa(\partial/\partial x) \times \langle T \rangle$  the mixing will effectively be sufficient to maintain the TEP profiles. On the other hand, the viscous flux will dominate if the turbulence is suppressed.

The generation of the poloidal flow is described by the Reynolds stress. This is seen by averaging Eq. (3) over  $y$  to obtain the equation for the evolution of the poloidal velocity,

$$\frac{\partial V}{\partial t} = - \frac{\partial}{\partial x} \langle uv \rangle + \mu \frac{\partial^2}{\partial x^2} V, \tag{14}$$

where  $v$  is the poloidal velocity component and  $V = \langle v \rangle$ . The Reynolds-stress,  $R_{uv} = \langle uv \rangle$ , which is the flux of momentum, is related to the turbulence level. However, a simple

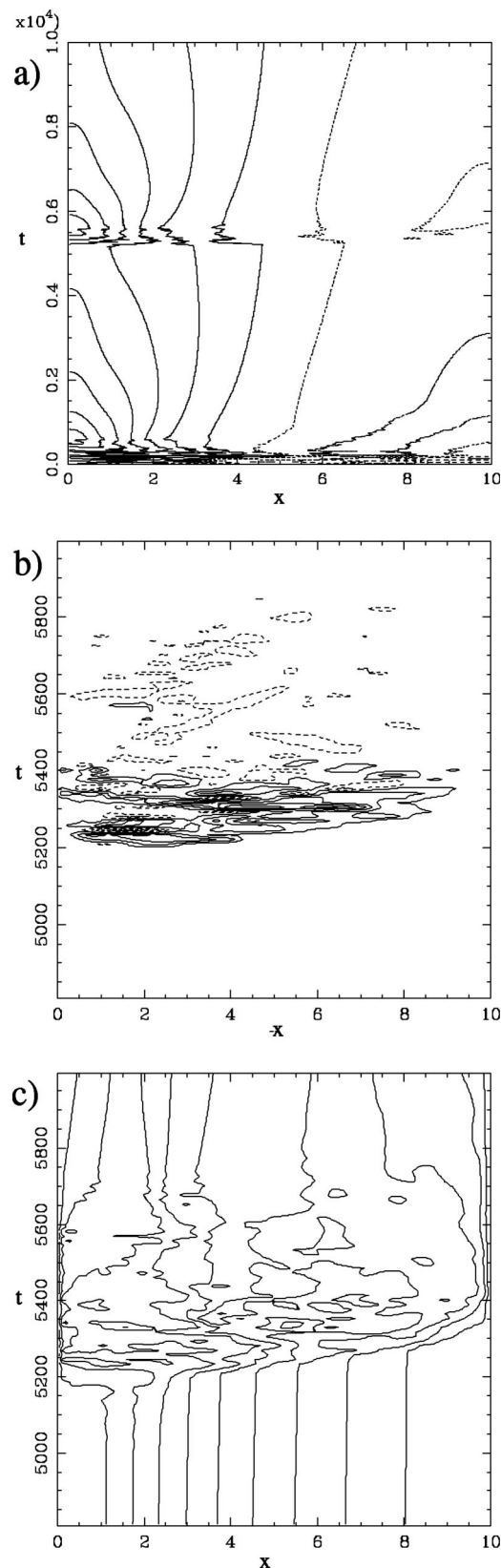


FIG. 3. (a) Contours of the poloidal velocity vs time and radial coordinate with contour levels spaced at intervals 0.2. (b) and (c) are enlarged with respect to time at the occurrence of the flux burst: (b)  $\Gamma_T(t)$  plotted vs  $(x, t)$  with  $dz=0.5$  and (c) the temperature profile vs time with contour spacing of  $dz=1$ . Same parameters were used for the run as in Fig. 2.

quasilinear estimate using the linear local dispersion relation does not give a contribution to  $R_{uv}$ , a seed poloidal flow or higher order nonlinear couplings are essential (see Appendix). Thus, when the turbulence is quenched the lower level turbulence is increasingly unable to transport momentum into the flow, and the poloidal flow will decay due to the viscosity. After the flow has decayed sufficiently and the pressure gradient have built up, the basic instability may develop again, resulting in a strong burst of turbulence and heat flux. We should emphasize that the heat flux in the fully developed turbulent case is always stronger than the momentum flux. Thus, the TEP state is established before the momentum flux has build up the poloidal flow.

This behavior is further detailed in Fig. 3, for the same parameters as in Fig. 2(a). Here we depict the evolution of the poloidal flow by showing the contours of  $V$  in the  $x-t$ -plane in Fig. 3(a). After the initial phase where the turbulence develops and establishes the TEP profiles a poloidal flow is seen to form at  $t \approx 100$ . The flow is strongest at the heated boundary where it is in the positive  $y$ -direction. Near the other wall it is reversed, resulting in a strong shear. This flow dominates the evolution for a long period, during which the turbulence is suppressed and the heat flux is negligible, compare Fig. 2(a). The poloidal flow is slowly decaying and at around  $t=5200$  it has become weak enough for allowing the onset of the instability and turbulence due to the built-up temperature profile. If the viscosity is larger, the poloidal flow decays faster, and the turbulent bursts are therefore more frequent, as in Fig. 2(b). Note that the linear growth rate of the Rayleigh–Taylor instability Eq. (10) for the present parameters is on the order of 0.1; which explains the fast growth of the turbulence. This leads to a burst in the heat flux and an associated flattening of the temperature profile as observed in Figs. 3(b) and 3(c). The flux is first established near the heated wall and the onset of the flux propagates outwards as a sharp front accompanied by the change in the temperature profile. Again a poloidal flow builds up at around  $t=5600$ . This quenches the turbulence and the flux and the previous scenario repeats.

#### IV. DISCUSSION OF SHEAR FLOW GENERATION

It remains to be explained why the poloidal flow is only dominating the evolution for aspect ratios below a critical value  $\alpha_c$ , which for the low viscosity case considered in Figs. 1–3 is approximately 3.8.  $\alpha_c$  depends on the viscosity, with a tendency to decrease with increasing viscosity.

In turbulent convection flows in neutral fluids governed by the Boussinesq equations Howard and Krishnamurti<sup>21</sup> described the generation of large scale flows by expanding the fields in only few fundamental modes and demonstrated that the poloidal flow mode ( $k=0$ ) could grow due to a “tilting” instability of the fundamental vortex-like modes. However, they did not address the influence of the aspect ratio. Basically their result shows that the growth of the shear flow is strongly dependent on the wave number ( $k=2\pi/L_y$  in our notations) of the fundamental mode, which was considered as the “pump” wave. The growth rate increases with  $k^2$  for smaller  $k$ -values ( $k \ll 2\pi/L_x$ ) and with  $k$  for larger values.

Drake *et al.*<sup>22</sup> applied a similar approach, to explain the formation of a global shear flow in the two-dimensional Navier–Stokes equations, they termed the instability: the “peeling” instability. However, they considered a different set of modes, ensuring that the total circulation ( $\int \Omega dx dy$ , where  $\Omega$  is the vorticity) is conserved. The instability was found to appear for an aspect ratio below  $\sqrt{5}$  in the case of weak dissipation. A similar result was recently obtained for the “resistive-g paradigm,”<sup>23</sup> i.e., RTI modes driven by only the “gravitational” coupling, by using a low-dimensional Galerkin approach. However, the appearance of a critical aspect ratio  $\alpha_c$  appears to be an artifact of the truncation into only few modes, as shown by Rosenbluth and Shapiro.<sup>24</sup> It is interesting to note that the results of Rosenbluth and Shapiro recovers the scaling of the growth rate with  $k^2$  for the small  $k$ -values, while for higher values (basically  $k \gg 1/L_x$ ) they find a periodic instability with comparatively much lower growth rate.

As stated above, we find in our simulations a clear critical aspect ratio. In the Appendix we have considered a simplified model for the shear flow generation again showing the very strong increase with  $k$  for small  $k$ 's. Expressing the growth rate,  $\gamma_V$ , in terms of  $\alpha$  (A6) we observe that  $\gamma_V$  decrease with  $\alpha$ , which agrees with the observations in Fig. 1, the time scale for the growth of the shear flow to suppress the turbulence is increasing with  $\alpha$ . For a sufficiently high value  $\alpha_c$  the growth rate can no longer overcome the viscous damping, and we believe that this is the course of the critical aspect ratio in our simulations. We also note that even if we have not yet performed a detailed parameter study of the dependence of  $\alpha_c$  on  $\mu$  it appears that  $\alpha_c$  decreases with increasing  $\mu$ .

We illustrate the mechanism of the flow generation for low aspect ratios by comparing the evolution of the vorticity field for the cases  $\alpha=2$  and  $\alpha=4$ . For the first case the quasistationary state, after the initial growth phase, is dominated by two counter rotating convective cells with superimposed short scale fluctuations, see Fig. 4. At the “borders” between the cells exist very concentrated outward streams of warm plasma and inward streams of cold plasma, i.e., the heat flux is spatially localized in thin channels, which are commonly observed in convection problems in neutral fluids. The borders are strongly wiggling with the largest amplitudes near the boundaries. The wiggling finally results in the squeezing of one of the convective cells at the expense of the other, and a global shear flow is established, manifesting the “tilting” instability.

In the case  $\alpha=4$  the initial evolution is similar, but now with four cells. This pattern also gets unstable and leaves two counter rotating cells, which are superimposed by relative weak poloidal flows forming and decaying roughly periodically. These flows are not sufficiently strong to shear apart the cell of the opposite vorticity, and the two-cell pattern survives. The periodically formed poloidal flows are observed to change direction between each period, and the flows ultimately vanish. Finally a very robust TEP state forms, where not only the temperature and density profiles follow the predicted TEP profiles, but also the potential vorticity profile  $\langle \Pi \rangle = \langle \nabla^2 \phi - \omega_B x - n \rangle$  approaches a constant

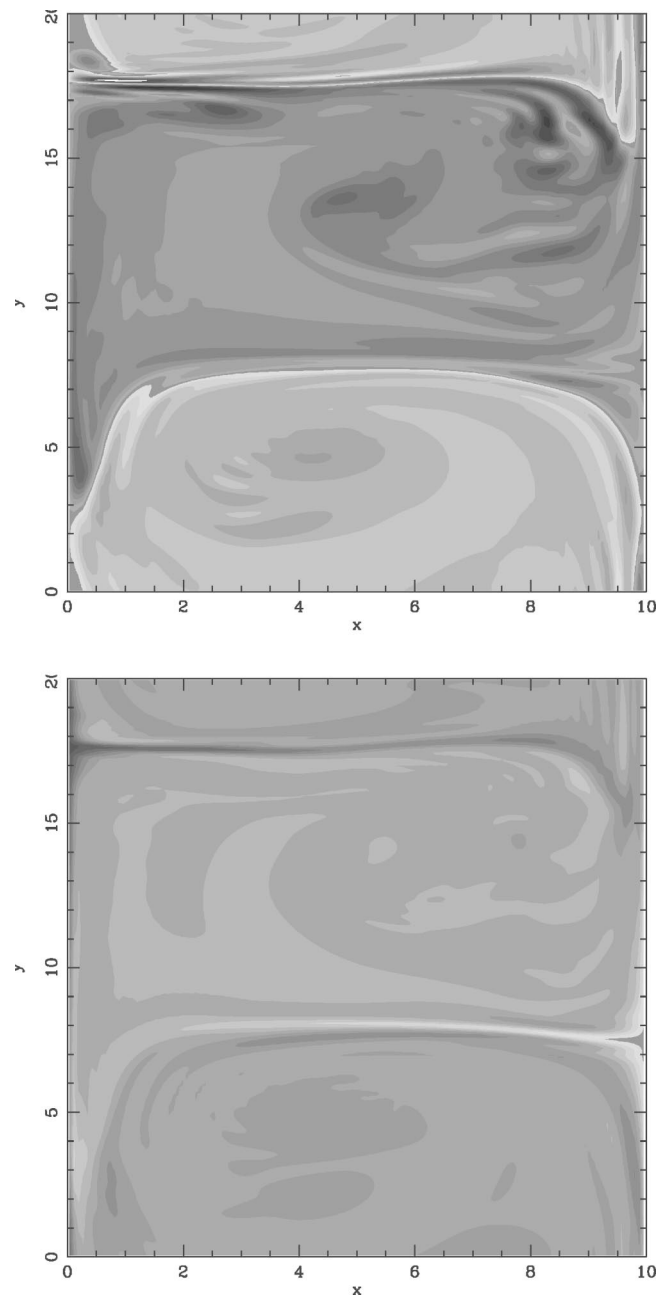


FIG. 4. The vorticity (gray scale between  $[-2:2]$ ) (top frame) and the temperature  $[-10:10]$  (bottom frame) before the transition to shear-flow for  $\alpha=2$  and  $\mu=10^{-3}$ . The system is heated at the left boundary with  $T_0=10$ .

value, implying that  $\langle \nabla^2 \phi \rangle = \langle n + \omega_B x \rangle + \text{const} = \text{const}$ . Note that there is a direct connection between the poloidal flow generation described by Eq. (14) and the equipartition of the potential vorticity  $\Pi$ . The flux of the vorticity  $\Omega = \nabla^2 \phi$  is given by  $\langle u \Omega \rangle = \partial_x R_{uv}$ , see also Ref. 25.

Once the poloidal flow is formed, it is observed that this flow appears to stabilize the steep supercritical (with respect to the RTI) pressure profile that builds up due to viscous diffusion in the quiet periods, see description of Fig. 3. This may be explained by the recent analysis of Benilov *et al.*<sup>26</sup> (see also Ref. 27), who demonstrates that an induced shear flow, irrespective of its actual profile, will tend to stabilize

the larger wave numbers of the RTI instability of an inversely stratified fluid. This implies that for a given geometry of the domain, i.e., a given aspect ratio, the shear flow may stabilize all the modes allowed by the geometry  $k > 2\pi/L_y$ . Thus, even if the shear flow is not stabilizing in the global sense<sup>28</sup> it may be stabilizing in a finite system. This may explain the long quiescent periods—the H-mode—with the steep gradients that we observe.

## V. CONCLUSION

In conclusion, we have shown that the nonlinear evolution of pressure driven turbulence in an inhomogeneous magnetic field depends strongly on the aspect ratio. We consider this as a crude but self-consistent and fully nonlinear model for turbulence on the outboard side of toroidal magnetic confinement devices. The aspect ratio in our model reflects the fact that when moving poloidally one will cross the same magnetic field line after some distance  $L$ . This sets an effective poloidal periodicity length assuming perfect correlation along magnetic field lines. For low aspect ratio, which would correspond to either high irrational  $q$  or  $q$  values close to rational ones, the evolution is characterized by long lasting quiescent H-mode periods with the turbulent transport suppressed by a poloidal shear flow that acts as a transport barrier. These periods are separated by short violent flux bursts (ELM) during which the poloidal flow breaks down. A similar behavior was also observed in toroidal gyrokinetic ion-temperature-gradient turbulence simulations, where the poloidal flows was damped by ion collisions.<sup>29,30</sup> For large aspect ratio we find a continuous strong turbulent flux, which, however, is temporally intermittent and spatially localized in narrow channels between the dominating convective rolls.

We have only considered specific typical cases in this work with the aim of bringing out the characteristic behaviors. We expect a very rich dynamical behavior when exploiting the full parameter diagram, in particular the role of the initial pressure gradient and the viscosity and diffusivities deserves a much more detailed analysis.

Although the model is simplified and lacks some geometrical effects, it contributes to the fundamental understanding of the role of poloidal flows in controlling turbulence and confinement and shows their fundamental relationship to the giant ELM type behavior observed in the H-mode. It reproduces the spatial and temporal intermittent evolution of the turbulent fluxes generally observed and offers a consistent nonlinear picture of ELM behavior, allowing some prediction of transport barrier formation in relation to the  $q$  profile. However, unless  $q$  is changed significantly this dependence might be weak. Additionally one should note that our values chosen for viscosity are rather high if compared with the edge region of a tokamak as discussed in Sec. III. We did find a tendency for a shift to higher critical aspect ratios  $\alpha_c$  for lower values of viscosities and diffusivities. Thus, at experimentally realistic viscosities/diffusivities we would expect  $\alpha_c$  to approach values more consistent with those estimated from experiment.

## ACKNOWLEDGMENTS

We thank Odd Erik Garcia for fruitful discussions on the shear flow generation.

This work was partly supported by the Danish Natural Sciences Foundation (SNF Grant No. 9903273).

## APPENDIX: QUASILINEAR ESTIMATION OF THE REYNOLDS STRESS

The poloidal flow generation is governed by Eq. (14). We attempt to estimate the Reynolds stress from a “quasilinear” approximation. When the wave field is represented in the form above Eq. (7) we find by direct calculation the contribution to poloidal flow acceleration,  $\partial_x \langle uv \rangle$ , from the  $k$ th wave-component,<sup>31</sup>

$$\partial_x \langle uv \rangle = -2k \partial_x (|\psi_k|^2 \partial_x \theta_k), \quad (\text{A1})$$

where  $\theta_k$  is the phase of  $\psi_k$ . We then use Eq. (7) and obtain, by multiplying by  $\psi_k^*$  and subtracting the complex conjugated equation multiplied by  $\psi_k$ ,

$$2 \partial_x (|\psi_k|^2 \partial_x \theta_k) + 2D_{\text{Im}} |\psi_k|^2 = 0, \quad (\text{A2})$$

and

$$\partial_x \langle uv \rangle = 2k D_{\text{Im}} |\psi_k|^2. \quad (\text{A3})$$

The requirement for a nonvanishing gradient in the Reynolds stress is that  $D_{\text{Im}} \neq 0$ . However, it is readily observed that in the local approximation  $D$  must be real. This also applies for the global modes, Eq. (11). Thus, the interaction of two waves that are governed by the dispersion relation will not contribute to a finite gradient in the Reynolds stress. However, if we assume that we have a small seed poloidal flow, i.e., we replace  $c$  by  $c - V$  in the expression for  $D$ , we get in the long wave limit,

$$D_{\text{Im}} \approx \frac{2UNc_i}{c_i^4}. \quad (\text{A4})$$

Considering the fundamental mode structure in the radial direction [ $n=1$  in Eq. (11)], which has the largest linear growth rate, we obtain  $c_i \approx \sqrt{|N|}/\sqrt{k^2 + \pi^2}$  as the long wave solution of the linear dispersion relation for  $N < 0$ . Inserting Eq. (A4) into Eq. (A3), and using Eq. (14) in the inviscid limit, we obtain the growth rate of  $V$ ,

$$\gamma_V = \frac{4k(k^2 + (\pi/L_x)^2)^{3/2}}{\sqrt{|N|}} |\psi_k|^2. \quad (\text{A5})$$

We now assume that the mode with  $k = 2\pi/L_y$  is dominating prior to the shear flow generation, which seems reasonable since the flow generation appears as the ultimate outcome of the inverse cascade. This is further equivalent to the analysis based on the few mode truncation, where the fundamental mode is considered as the “pump” wave (see the discussion in Sec. III). We introduce the aspect ratio  $\alpha = L_y/L_x$  in Eq. (A5) and obtain

$$\gamma_V = \frac{8\pi^4(4 + \alpha^2)^{3/2}}{L_x^4 \alpha^4 \sqrt{|N|}} |\psi_k|^2. \quad (\text{A6})$$

Thus, for the case of a fixed radial width the growth of the poloidal flow is decreasing with  $\alpha^4$  for  $\alpha \ll 2$ , while it decreases with  $\alpha$  for  $\alpha \gg 2$ . If we now account for the viscous dissipation of  $V$ , which gives an estimated damping rate as  $\mu(\pi/L_x)^2$ , then it is seen that for a certain value of  $\alpha$  the shear flow growth rate becomes too weak to overcome the damping, which may provide an explanation for the observed critical  $\alpha$ , and indeed  $\alpha_c$  is observed to decrease with increasing  $\mu$ .

<sup>1</sup>P. B. Rhines, *Annu. Rev. Fluid Mech.* **11**, 401 (1979).

<sup>2</sup>F. H. Busse, *Phys. Fluids* **14**, 1301 (2002).

<sup>3</sup>P. W. Terry, *Rev. Mod. Phys.* **72**, 109 (2000).

<sup>4</sup>F. Wagner and U. Stroth, *Plasma Phys. Controlled Fusion* **35**, 1321 (1993).

<sup>5</sup>K. H. Burrell, *Phys. Plasmas* **6**, 4418 (1999).

<sup>6</sup>F. Wagner, G. Becker, and K. Behringer, *Phys. Rev. Lett.* **49**, 1408 (1982).

<sup>7</sup>The Asdex Team, *Nucl. Fusion* **29**, 1959 (1989).

<sup>8</sup>H. Zohm, *Plasma Phys. Controlled Fusion* **38**, 105 (1996).

<sup>9</sup>W. Suttrop, *Plasma Phys. Controlled Fusion* **42**, A1 (2000).

<sup>10</sup>P. H. Diamond and Y. B. Kim, *Phys. Fluids B* **3**, 1626 (1991).

<sup>11</sup>H. Biglari, P. H. Diamond, and P. W. Terry, *Phys. Fluids B* **2**, 1 (1990).

<sup>12</sup>V. Naulin, J. Nycander, and J. Juul Rasmussen, *Phys. Rev. Lett.* **81**, 4148 (1998).

<sup>13</sup>V. V. Yankov and J. Nycander, *Phys. Plasmas* **4**, 2907 (1997).

<sup>14</sup>P. H. Diamond and T.-S. Hahm, *Phys. Plasmas* **2**, 3640 (1995).

<sup>15</sup>A. Takayama, M. Wakatani, and H. Sugama, *Phys. Plasmas* **3**, 3 (1996).

<sup>16</sup>D. J. Tritton, *Physical Fluid Dynamics*, 2nd ed. (Clarendon, Oxford, 1988).

<sup>17</sup>A. Arakawa, *J. Comput. Phys.* **1**, 119 (1966).

<sup>18</sup>G. E. Karniadakis, M. Israeli, and S. A. Orszag, *J. Comput. Phys.* **97**, 414 (1991).

<sup>19</sup>H. R. Wilson, P. B. Snyder, G. T. A. Huysmans, and R. L. Miller, *Phys. Plasmas* **9**, 1277 (2002).

<sup>20</sup>P. B. Snyder, H. R. Wilson, J. R. Ferron *et al.*, *Phys. Plasmas* **9**, 2037 (2002).

<sup>21</sup>L. N. Howard and R. Krishnamurti, *J. Fluid Mech.* **170**, 385 (1986).

<sup>22</sup>J. F. Drake, J. M. Finn, P. N. Guzdar *et al.*, *Phys. Fluids B* **4**, 488 (1992); J. M. Finn, J. F. Drake, and P. N. Guzdar, *ibid.* **4**, 2758 (1992).

<sup>23</sup>M. Berning and K. H. Spatschek, *Phys. Rev. E* **62**, 1162 (2000).

<sup>24</sup>M. N. Rosenbluth and V. D. Shapiro, *Phys. Plasmas* **1**, 222 (1994).

<sup>25</sup>V. Naulin, *Europhys. Lett.* **43**, 533 (1998).

<sup>26</sup>E. S. Benilov, V. Naulin, and J. Juul Rasmussen, *Phys. Fluids* **14**, 1674 (2002).

<sup>27</sup>H. L. Kuo, *Phys. Fluids* **6**, 195 (1963); A. B. Hassam, *Phys. Fluids B* **4**, 485 (1992).

<sup>28</sup>J. W. Miles, *J. Fluid Mech.* **10**, 496 (1961); L. N. Howard, *ibid.* **10**, 509 (1961).

<sup>29</sup>Z. Lin, T. S. Hahm, W. W. Lee, W. M. Tang, and P. H. Diamond, *Phys. Rev. Lett.* **83**, 3645 (1999).

<sup>30</sup>M. A. Malkov, P. H. Diamond, and M. N. Rosenbluth, *Phys. Plasmas* **8**, 5073 (2001).

<sup>31</sup>H. Sugama and W. Horton, *Phys. Plasmas* **1**, 345 (1994).